Journal of Power Sources 195 (2010) 4736–4742

Contents lists available at ScienceDirect

Journal of Power Sources

journal homepage: www.elsevier.com/locate/jpowsour

Measurement of internal wettability of gas diffusion porous media of proton exchange membrane fuel cells

B.R. Friess, M. Hoorfar*

University of British Columbia Okanagan, Kelowna, BC, Canada V1V 1V7

ARTICLE INFO

Article history:
Received 11 January 2010
Received in revised form 26 February 2010
Accepted 1 March 2010
Available online 6 March 2010

Keywords:
Gas diffusion layer
Wettability
Surface energy
Capillary height penetration technique
Washburn's equation
Owens–Wendt surface tension model
Equation-of-state approach

ABSTRACT

One of the major problems of current proton exchange membrane (PEM) fuel cells is water management. The gas diffusion layer (GDL) of the fuel cell plays an important role in water management since humidification and water removal are both achieved through the GDL. Various numerical models developed to illustrate the multiphase flow and transport in the fuel cell. The accuracy of these models depends on the accurate measurement of the GDL properties such as wettability, surface energy, and porosity. Most of the studies conducted for measuring the wettability of the GDL are based on the external contact angle measurements. However, the external contact angle does not describe adequately capillary forces acting on the water inside the GDL pores. In a recent study, the capillary penetration technique has been used to measure indirectly the wettability of the GDL based on the experimental weight increase due to penetration of the liquid into the porous sample. In essence, the mass penetration technique was used along with the Washburn's equation. The shortcoming of this method is that the external factors such as the mass of the meniscus formed outside the sample as well as evaporation occurring during the experiment were not considered. It was found that these factors affect the wettability measurements of the GDL, especially for a hydrophilic sample. In this paper, the experimental setup of the capillary penetration method has been modified to control the evaporation rate as the liquid is penetrated into the sample. Also, the capillary penetration technique which was initially used based on mass penetration has been modified to the height penetration method to eliminate the effect of the weight of the meniscus formed outside the sample. The experiments were performed for a time period of 10 s. For this time period, it was found that the Washburn's equation is not an accurate model since it does not include the frictional work effects that are significant at the first few seconds of the experiments. Therefore, the Washburn's equation was replaced by a more general form. Using the Levenberg–Marquardt optimization technique, the experimental data obtained from the height penetration technique is fitted to the theoretical curve to find the internal contact angles of a sample GDL. Finally, these contact angle results are used to determine the surface tension of the GDL using two approaches: the Owens–Wendt surface tension components and the equation-of-state models.

1. Introduction

Proton exchange membrane (PEM) fuel cells have drawn much attention in the last decade as a high-efficiency and low-emission source of energy for industrial products ranging from vehicles to portable electronic devices. However, the performance and cost of the PEM fuel cells must be improved before they can constitute a viable market and replace current battery technologies. The PEM fuel cell consists of a membrane electrode assembly (MEA) sandwiched between two flow channels. The MEA contains a polymer electrolyte membrane (e.g. Nafion) embedded between two porous gas diffusion electrodes (GDE). The GDE is composed of a platinum catalyst and a gas diffusion layer (GDL) constructed from macroporous substrates (i.e., carbon fiber or carbon cloth impregnated with polytetrafluoroethylene (PTFE)) coated with one or more microporous layers (i.e., amorphous mixture of carbon and PTFE). Recent experimental and numerical investigations identify water management as a critical factor in the design of robust and high-efficiency fuel cells [1–7]. In essence, the polymer membrane of the PEM fuel cell needs to be well hydrated to maintain proton conductivity. However, excessive water vapor condensation, due to a long operation or large output current, forms microdroplets that cover the active sites on the catalyst layers, fills the pores of the GDL, and blocks access of the reactant gas to the reaction site [8]. Typically, this is the origin of the limiting current for PEM fuel cells. To enhance water management, it is necessary to study droplet formation and multiphase flow in the internal network of the

* Corresponding author at: School of Engineering, University of British Columbia Okanagan, Canada. Tel.: +1 250 807 8804; fax: +1 250 807 9850.
E-mail address: mina.hoorfar@ubc.ca (M. Hoorfar).

0378-7753/$ – see front matter
doi:10.1016/j.jpowsour.2010.03.001

Nomenclature

R	average pore radius
γ_{lv}	liquid surface tension
γ_{sl}	liquid–solid interfacial tension
γ_{sv}	solid surface tension
γ_d	dispersive component of surface tension
γ_p	polar component of surface tension
θ	average internal contact angle
g	gravitational constant
ρ	liquid density
η	liquid viscosity
A	wetted area
ε	porosity
t	penetration time
m	mass of capillary penetration
h	height of capillary penetration

fuel cell, especially through the GDL as humidification and water removal are both achieved through this porous medium. Experimental results obtained from a fluorescence microscopy technique show that water transport in the GDL is dominated by fingering and channeling effects which are dependent on the surface properties of the porous structure [9]. Also, in the models developed recently [10–13], the effects of the viscous and capillary forces as well as the porosity and wettability of the GDL on liquid water transport were elucidated. However, the wetting properties of the GDL were either approximated or measured using experimental methods such as the goniometry, capillary rise and Wilhelmy plate methods which only determine the external contact angles. The contact angle values of 120° (or even larger) have been reported for different GDLs using these external contact angle methods [13–18]. Since the contact angle of water on a pure PTFE surface is approximately 108°, these large values of contact angle cannot be due to the presence of the hydrophobic agent (PTFE) inside the GDL pores but rather due to surface roughness of the GDL. In general, the external contact angle may describe qualitatively the wettability of the GDL, but it cannot be used as a quantitative estimation for calculations or design purposes. Thus, it is required to find a method that is capable of measuring the internal wettability of the GDL.

The capillary penetration technique has been used to understand the relationship between pore structure, internal wettability and capillarity. In a recent study [19], this technique has been used to determine and further control the penetration of liquid into the GDL of the fuel cells. The modified Washburn's equation which relates the capillary to the viscous forces and neglects the effect of inertial and gravitational forces has been used to measure the internal contact angle from the penetration rate of liquid into the porous media [19]. The modified Washburn's equation is given as

$$m^2 = \frac{\eta \cos\theta}{\gamma_{lv}\rho C_w} t \quad (1)$$

where m is the mass of the sample liquid penetrated into the GDL, θ is the average internal liquid contact angle formed by the liquid and the GDL material, γ_{lv} is the liquid–vapor surface tension, ρ is the density of the sample liquid, η is the viscosity of the sample liquid, and C_w presents the Washburn's constant of the GDL sample which is assumed to be material dependent and a function of the GDL pore structure (e.g., mean pore diameter (R) and porosity (ε)).

The determination of the contact angle values using the modified Washburn's equation involves the following steps: (1) the GDL sample is first tested with a sample liquid that is assumed to have a zero-contact angle (i.e., $\cos\theta = 1$) to the GDL pores (e.g., pentane); (2) the experimental weight increase due to penetration

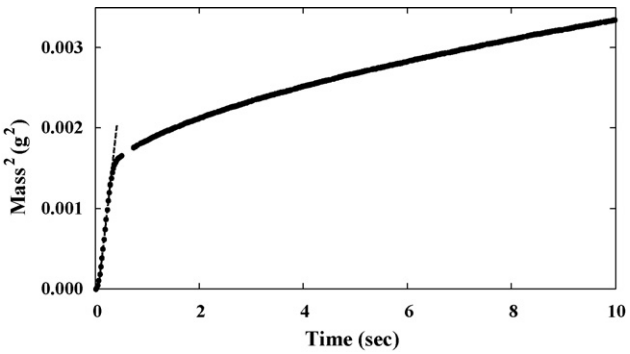

Fig. 1. This figure presents the mass-squared-versus-time plot for a sample GDL in contact with pentane. The modified Washburn's question (Eq. (1)) was fitted to the first linear portion of the experimental weight increase curve.

is measured over time; (3) the mass-squared-versus-time plot is obtained (Fig. 1 presenting a typical graph); (4) knowing the properties of the zero-contact angle liquid, the slope of the linear section (the first part of the mass-squared-versus-time plot) will determine the Washburn's constant (C_w); (5) with the Washburn's constant determined, contact angle against other different sample liquids are measured using the slope of the linear portion of the mass-squared-versus-time plot obtained for other sample liquids. The results obtained from this approach show that for some testing liquids the values of contact angle are not defined ($\cos\theta > 1$). This can be due to the fact that the contact angles were determined using the modified Washburn's equation, which neglects the effect of the gravitational and inertial forces, and considering only the first portion of the experimental weight increase data. The results reported by Hamraoui and Nylander [20] show that the effect of the gravitational and inertial forces is comparable to that of capillary and viscous forces, especially at the early stage of penetration. In our initial attempt [21], the complete form of the Washburn's equation (Eq. (2)) was used to include the above effects.

$$\underbrace{\frac{2}{R}\gamma_{lv}\cos\theta}_{\text{surface tension}} = \underbrace{\frac{g}{\rho A \varepsilon} m}_{\text{gravity}} + \underbrace{\frac{8\eta}{R^2A^2\rho^2\varepsilon^2} m\frac{dm}{dt}}_{\text{viscosity}} + \underbrace{\frac{1}{\rho A^2\varepsilon^2}\frac{d}{dt}\left(m\frac{dm}{dt}\right)}_{\text{inertia}} \quad (2)$$

where g is the gravitational constant, and R, ε, and A present the mean pore diameter, porosity, and wetted area, respectively.

Since the GDL samples are partially hydrophobic (due to PTFE loadings) mass penetration experiments were conducted using sample liquids such as methanol, acetone, cyclohexane, chloro-

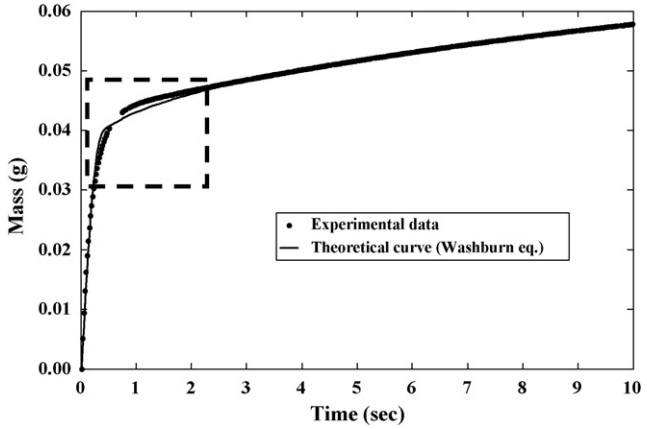

Fig. 2. In this figure, the theoretical curve obtained by integrating the complete Washburn's equation (Eq. (2)) was fitted to the entire experimental weight increase curve which was obtained for pentane.

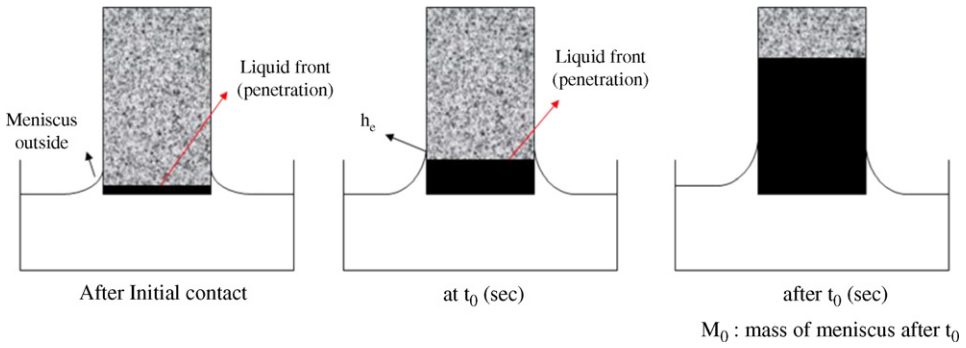

Fig. 3. The schematic representation of the capillary penetration (inside the sample) and the meniscus rise (outside the sample) phenomena.

form, and toluene. This method does not require the calculation of C_w (Washburn's constant). Thus, it is not required to use a sample liquid such pentane which is assumed to wet completely the GDL sample. Fig. 2 presents the results of the experimental weight increase of a GDL sample due to penetration of a test liquid and the best fitted theoretical curve (obtained by integrating the complete form of the Washburn's equation).

The fit is good except for the first few seconds of the experiment. It has been shown [22] that during this short period of time the weight increase is a result of two simultaneous phenomena: the capillary penetration inside the GDL, and the formation of meniscus outside the sample. The formation of the meniscus outside can be seen schematically in Fig. 3. During the first few seconds of the experiment the meniscus mass is the dominant factor until time t_0 where the meniscus reaches an equilibrium height h_e. After time t_0 capillary penetration becomes the dominant factor especially for hydrophobic surfaces for which the penetration from the outside meniscus to the inside layers is not as significant as the imbibition phenomenon. It is necessary to separate the mass increase due to two phenomena in order to achieve the meaningful contact angle values. This was achieved by fitting the Washburn's equation to the data after the sharp "corner" in the mass-versus-time graph [21]. The fitted curve was than integrated over the entire time interval to obtain the theoretical mass increase due to capillary penetration (see Fig. 4). This mass can then be used to find the weight increase due to the meniscus by subtracting the capillary mass from the experimental mass values in the first few seconds of the experiment (where the meniscus factor is most prevalent) (see Fig. 5). This procedure was repeated for different sample liquids. The results are listed in Table 1. At first glance, these values are realistic compared to those obtained from the previous approach as this method measures the average internal contact angles using the complete form of the Washburn's equation.

Table 1
Internal contact angle values obtained for a sample GDL using the capillary mass-based penetration technique in conjunction with the Washburn's equation.

Test liquid	γ_{lv} (mJ m^{-2})[a]	θ (deg.)[b]
Methanol	22.7	34.3
Acetone	23.7	29.2
Cyclohexane	25.5	41.2
Chloroform	27.2	47.5
Toluene	28.4	50.8

[a] These values were obtained from [23].
[b] These contact angle values were obtained by fitting Eq. (2) to the mass penetrated experimental data.

The above method was applied to a hydrophilic GDL sample (with 10 wt.% or less PTFE loading). The contact angle results obtained for a hydrophilic GDL, however, were not valid ($\cos\theta > 1$). This can be due to the fact that the meniscus formed outside the GDL wall penetrates into the internal layers before reaching to the equilibrium height (h_e). Thus, it is impossible to separate the effect of the weight increase due to imbibition from that of the meniscus outside. As a result, the mass penetration method explained above fails to determine correct contact angle values, especially for hydrophilic porous samples.

In this work, the capillary penetration technique based on height of penetration was used instead of the mass penetration method. The experimental setup was further improved to eliminate the effect of evaporation. The experiments were conducted for hydrophilic GDL samples and repeated for several pure liquids. The details of the material and method are explained in Section

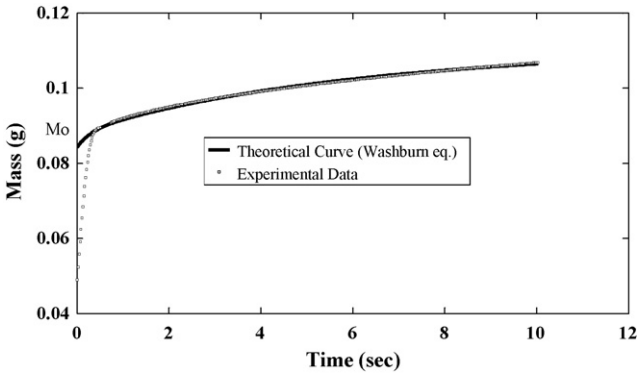

Fig. 4. The complete Washburn's curve (obtained by integrating Eq. (2)) was fitted to a portion of the experimental weight increase curve (obtained for pentane) to separate the effect of the capillary penetration from the meniscus formed outside the GDL sample.

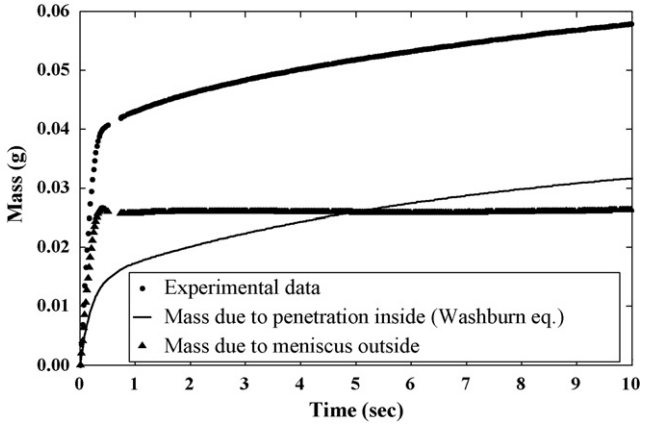

Fig. 5. The effect of the meniscus outside and the sample liquid (pentane) penetration inside the GDL is separated. The solid line is the theoretical curve which was obtained by integrating the complete Washburn's equation (Eq. (2)).

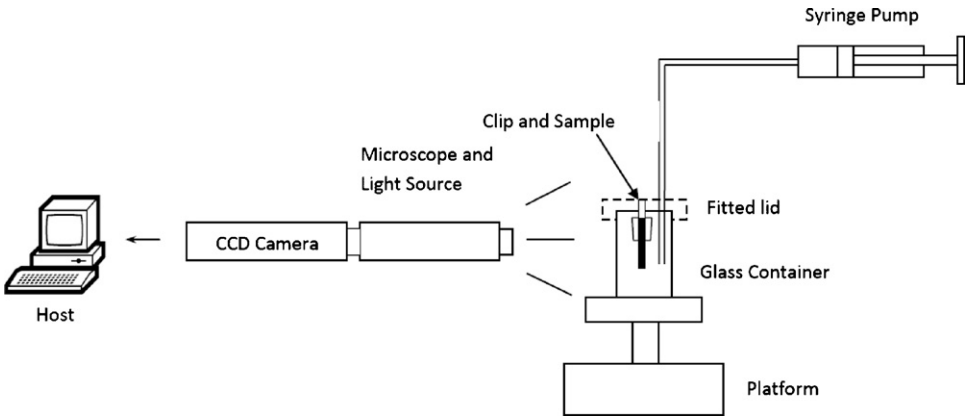

Fig. 6. The schematic representation of the experimental setup for the capillary penetration height experiment.

2. Also, a more general form of Washburn's equation has been used (instead of Eq. (2)) to include frictional work effects which are significant at short time periods. The experimental data obtained from the height penetration method was fitted to the new equation using the Levenberg–Marquardt optimization method (see Section 3). The best fit determines the value of the internal contact angle for each sample liquid (see Section 4). Finally, the internal contact angle results obtained from a variety of test liquids are used to determine the wettability and surface tension of the sample GDL using two approaches: the Owens–Wendt two-parameter and the equation-of-state approaches (explained in Section 4).

2. Materials and method

The objective of this study is to find the wettability (i.e., the internal contact angle of water in the pores of the GDL) and surface tension of the GDL porous media. However, water cannot be used as the test liquid in the capillary penetration technique since the GDL samples are partly hydrophobic. In this work, the capillary penetration experiments are conducted with a set of pure liquids to find their internal contact angles in the sample GDL material. Later on, these internal contact angle values are used to determine the wettability and surface energy of the GDL using two models: the surface tension components and the equation-of-state approaches.

Toray TGP-H-120 (10 wt.% PTFE loading) nonwoven fibrous gas diffusion layer (GDL) samples were used. The set of test liquids used in this study includes hexane, heptanes, ethanol, methanol, acetone, cyclohexane, and toluene. All test liquids (with purity greater than 99.9%) were supplied from Sigma–Aldrich. The height increase was measured using an optical setup that includes an APO Zoom Leica microscope connected to a digital camera and a sealed container containing the liquid and the GDL sample. The container is sealed with a fitted PDMS lid with two openings. One of the openings is to secure the clip that holds the GDL to the PDMS lid. The second opening allows the user to dispense enough liquid to raise the liquid level until it contacts the GDL sample. Fig. 6 presents the schematic representation of the setup.

The experiment was completed in two steps: First, the sample liquid is dispensed into the container and left for a while to saturate the air inside the container. Then, before starting the experiment, more liquid is injected into the container until the liquid level reaches the GDL sample. This way the effect of evaporation is minimized. As the liquid sample penetrates into the GDL, the images are acquired with a high resolution camera at a rate of 20 frames per second. Fig. 7 shows the images of height of penetration acquired in a typical experiment. The images were finally processed using an image analysis software program developed to obtain the height-versus-time curve.

3. Theory and calculation

3.1. General capillary penetration equation

The modified Washburn's equation, which relates the effect of surface tension and viscous forces without considering gravitational and inertial forces, has been used to find the wettability of porous media [19,24–26]. The integration of the modified Washburn's equation results in a simple relation that predicts a linear behavior when the square of the increase of weight of the porous solid due to liquid penetration is plotted as a function of time. Thus, the internal contact angles presented in [19,24–26] were obtained by fitting a straight line to only a first few seconds of the mass-squared-versus-time plot since the deviation of the experimental data from the theoretical Washburn's curve grow dramatically after the first few seconds. This significant deviation is because of neglecting the gravity an inertial terms that are present in the complete form of the Washburn's equation (Eq. (2)). Preliminary results, however, showed that for experiments conducted at short time periods the Washburn's equation (Eq. (2)) is not an accurate model. This is due to the fact that the Washburn's equation (Eq. (2)) is derived based on a quasi-steady-state approximation in which the kinetic energy and the frictional work within the fluid are neglected [27]. This renders the Washburn's equation inadequate for short times when the liquid momentum changes rapidly with time and height of penetration. Consideration of energy conservation and frictional work gives a more general and rigorous hydrodynamic equation (see Eq. (3)) for the penetration of a fluid into a porous sample [27]. At short times, the general equation (Eq. (3)) and the Washburn's equation (Eq. (2)) are quite different. At long time periods, the two equations merge together. In other words, the Washburn's equation is only an asymptotic solution, not valid for short time.

$$\frac{1}{\rho}\left(\frac{2}{R}\gamma_{lv}\ \cos\theta - \rho g h\right) = \left(h + \frac{7}{6}R\right)\frac{d^2h}{dt^2} + 1.225\left(\frac{dh}{dt}\right)^2 + \frac{8\eta h}{(\rho R)^2}\frac{dh}{dt} \tag{3}$$

An efficient optimization method (explained in Section 3.2) is used to determine the internal contact angle values based on the best fit between the experimental data and the theoretical curve obtained by integrating Eq. (3). The integration is performed using Runge–Kutta method. The second order nonlinear ODE Eq. (3) is converted into the following set of first order nonlinear ODE equa-

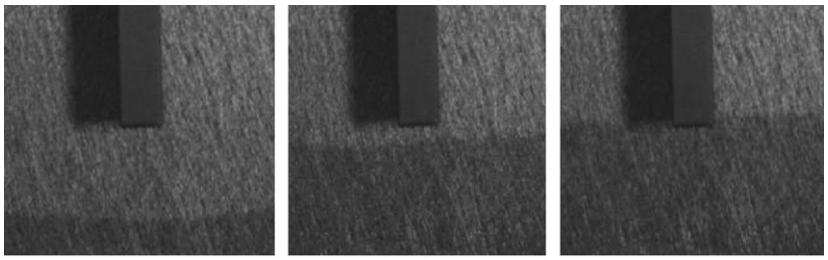

Fig. 7. Images of capillary height penetration acquired at three time intervals for the sample liquid of hexane.

tions:

$$\begin{cases} y_1' = y_2 \\ y_2' = \dfrac{1}{\rho}\dfrac{((2\gamma a/b) - \rho g h)}{(y_1 + (7/6)b)} - \dfrac{1.225 y_2^2}{(y_1 + (7/6)b)} - \left(\dfrac{8\eta}{\rho b^2}\right)\dfrac{y_2}{(y_1 + (7/6)b)} \end{cases} \tag{4}$$

where $y_1 = h$, $y_2 = h(dh/dt)$, $a = \cos\theta$ and $b = R$ (a and b are the optimization parameters).

For known liquid properties (i.e., liquid density, viscosity and surface tension), the best fit between the experimental and theoretical curves will determine not only the internal contact angle but also the average pore size of the porous media.

3.2. Optimization procedure

To evaluate the agreement between the experimental data and the theoretical curve, an objective function, E, is defined as the sum of the individual errors, e_i, given as

$$E = \sum_{i=1}^{N} e_i \tag{5}$$

$$e_i = (y - Y)^2 \tag{6}$$

where y and Y present the theoretical and experimental height, respectively. The objective function, E, is a function of a set of parameters p, with elements p_k, $k = 1, \ldots, M$. The goal is to find the parameter set p that gives the best fit between the experimental points and a theoretical curve. The objective function, E, will assume a single absolute minimum value at one point in the M-dimensional space of E. In this study, p is the vector of two parameters (i.e., $p = [a\ b]^{\mathrm{T}}$). To find the best fit between the experimental points and the theoretical curve, the objective function must be minimized. The necessary conditions for an extremum in the value of E are

$$\frac{\partial E}{\partial p_k} = \sum_{i=1}^{N} \frac{\partial e_i}{\partial p_k} = 0, \quad k = 1, \ldots, M \tag{7}$$

These extremum conditions form a set of algebraic equations in the variables p_k, $k = 1, \ldots, M$. An iterative solution is required to solve for these variables. There exist several methods to solve these systems of equations. There are no general or perfect methods for solving systems of nonlinear equations. Every method has advantages and disadvantages, and the choice of a particular method depends on the characteristics of the problem. The best known and most powerful one is the Newton–Raphson method [28]. This method is very easy to implement and its asymptotic convergence rate is quadratic. However, it requires a good initial estimate of the optimization parameters. In this study, the Levenberg–Marquardt method [28] was used to solve the system of Eqs. (7) since it maintains global convergence while providing a similar convergence rate to the Newton–Raphson method. The iterative procedure of Levenberg–Marquardt method can be expressed as

$$p^{i+1} = p^i - \Delta p^i \tag{8}$$

where p^i is the vector of unknown variables at the ith iteration step and Δp^i is a correction vector resulting from the solution of the associated linear system.

$$(H(p^i) + \lambda_k I) \times \Delta p^i = E(p^i) \tag{9}$$

The components of the vector $E(p^i)$ are the first partial derivative terms obtained from Eq. (7) and evaluated at the ith step. λ_k is a user defined correction factor that increases if the error in a step increases (approaching the solution to the global line search method) or decrease when the error decreases (approaching the solution to the Newton–Raphson method). The Hessian matrix $H(p^i)$ is a symmetric matrix whose components are computed as follows:

$$\frac{\partial^2 E}{\partial p_k \partial p_l} = \sum_{i=1}^{N} \frac{\partial^2 e_i}{\partial p_k \partial p_l} \tag{10}$$

One important advantage of this algorithm is that the value of the objective function and its first and second partial derivatives are all evaluated with the same degree of accuracy, since they can be evaluated analytically in terms of first order ordinary differential expressions that can be integrated numerically. The initial values of the parameters are estimated using a Monte Carlo method which alters initial values for $p = [a\ b]^{\mathrm{T}}$ by random amounts over numerous iterations until an error of 10^{-3} has been achieved. To refine each optimization parameters and enhance convergence, the incremental loading method [28] was combined with the Levenberg–Marquardt technique. In general, convergence is completed once an error of 10^{-6} or less was achieved.

4. Results and discussion

The optimization method explained in the previous section was used to determine the internal contact angle for the test liquids. Fig. 8 presents the result of the experimental data obtained from the capillary height penetration method and the best fitted theoretical curve generated by integrating Eq. (3).

The experiments were conducted for different test liquids to calculate their internal contact angles. These results are summarized in Table 2. For each liquid the experiments were repeated three times, each time with a new GDL sample. The error limits of the contact angle values were obtained with a 95% confidence level.

The internal contact angle values presented in Table 2 were used to calculate the wettability and surface energy of the sample GDL using two approaches: Owens–Wendt surface components and equation-of-state approaches.

Table 2
Contact angle values obtained for Toray TGP-H-120 (10 wt.% PTFE loading) samples.

Test liquid	γ_{lv}^{p} (mJ m^{-2})[a]	γ_{lv}^{d} (mJ m^{-2})[a]	γ_{lv} (mJ m^{-2})[a]	ρ (g cm^{-3})[a]	η (mPa s)[a]	θ (deg.)[b]
Hexane	0.0	18.43	18.43	0.6548	0.308	14.2 ± 0.6
Heptane	0.0	20.14	20.14	0.6837	0.379	27.8 ± 0.5
Ethanol	8.3	14.0	22.3	0.789	1.160	37.7 ± 0.4
Methanol	6.7	16.0	22.7	0.792	0.577	39.2 ± 0.2
Acetone	6.4	17.3	23.7	0.791	0.326	42.6 ± 0.8
Cyclohexane	0.0	25.5	25.5	0.779	0.980	47.7 ± 0.9
Toluene	2.3	26.1	28.4	0.867	0.590	54.5 ± 0.7

[a] These values were obtained from [23].
[b] These contact angle values were obtained by fitting Eq. (3) to the height penetrated experimental data.

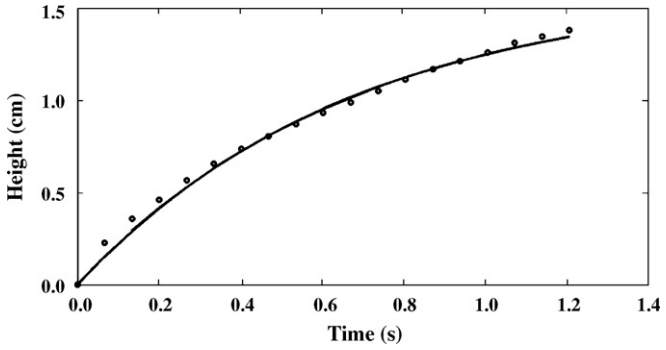

Fig. 8. The best fit between the experimental height penetration rate (obtained for hexane) and the theoretical curve obtained by integration the general equation (Eq. (3)).

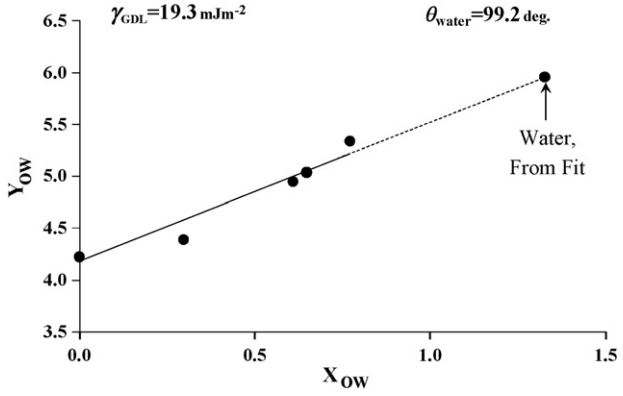

Fig. 9. The wettability and surface tension of the GDL using the surface components approach.

4.1. Owens–Wendt two-parameter model

According to the Owens–Wendt two-parameter model [19] (Eq. (11)), liquid and solid surface tensions consist of two components: dispersive and polar parts. In Eq. (11), the two unknown components of the GDL surface tension (γ_{sv}^{d}, γ_{sv}^{p}) can be determined from the previously measured contact angles against the sample liquids with known values of surface tension components (γ_{lv}^{d}, γ_{lv}^{p}).

$$\underbrace{(1+\cos\theta)\left((\gamma_{lv}^{p}+\gamma_{lv}^{d})/2\sqrt{\gamma_{lv}^{d}}\right)}_{Y_{OW}} = \underbrace{\sqrt{\gamma_{sv}^{d}}}_{A} + \underbrace{\sqrt{\gamma_{sv}^{p}}}_{B}\cdot\underbrace{\sqrt{\gamma_{lv}^{p}/\gamma_{lv}^{d}}}_{X_{OW}} \quad (11)$$

A plot of Y_{OW} versus X_{OW} for different liquids yields the dispersive components γ_{sv}^{d} (square of the y-intercept), the polar component γ_{sv}^{p} (square of the slope) and consequently the surface tension of the GDL. For the known value of $\sqrt{\gamma_{lv}^{p}/\gamma_{lv}^{d}}$ for water, the internal contact angle of water in the GDL pores can be calculated from the ordinate after extrapolation. Fig. 9 represents the results obtained using this method. The internal contact angle of water and surface energy of the sample GDL determined using this method are 99.2° (deg.) and 19.3 mJ m^{-2}, respectively.

4.2. Equation-of-state approach

According to the equation-of-state approach [29], the values of $\gamma_{lv}\cos\theta$ vary systematically with γ_{lv} in a very regular fashion, from hydrophobic surfaces (such as polytetrafluoroethylene) to hydrophilic surfaces (such as polypropene-alt-*N*-methylmaleimide) and that the patterns are independent of the experimental technique. Thus, one can conclude that the values of $\gamma_{lv}\cos\theta$ depend only on γ_{lv} and γ_{sv} (i.e., $\gamma_{lv}\cos\theta$ is a function of γ_{lv} and γ_{sv}). Because of Young's equation (Eq. (12)), the experimental contact angles imply that γ_{sl} can be expressed as a function of only γ_{lv} and γ_{lv}.

$$\gamma_{lv}\cos\theta = \gamma_{sv} - \gamma_{lv} \quad (12)$$

Based on the above statement, a recent formulation of the equation-of-state approach was written as

$$\gamma_{sl} = \gamma_{sv} + \gamma_{lv} - 2\sqrt{\gamma_{lv}\gamma_{sv}}e - \beta(\gamma_{lv}-\gamma_{sv})^2 \quad (13)$$

Combining Eq. (13) with the Young's equation (12) yields

$$\sqrt{\gamma_{lv}}(1+\cos\theta) = 2\sqrt{\gamma_{sv}}e^{-\beta(\gamma_{lv}-\gamma_{sv})^2} \quad (14)$$

The solid surface tension (γ_{sv}) and β can be calculated from experimental contact angles and liquid surface tensions. In this paper, the surface tension of the GDL samples was obtained using this approach. The surface tension of the liquid samples and their corresponding contact angles listed in Table 2 (measured from the capillary height penetration method) were used to calculate the surface energy of the GDL sample. Fig. 10 presents the experimental points fitted to Eq. (14). The Levenberg–Marquardt optimization

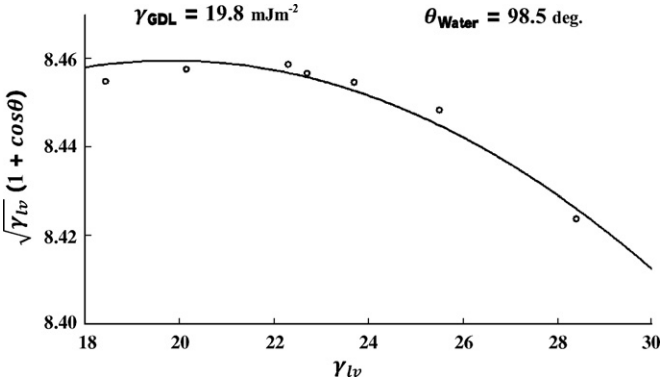

Fig. 10. The wettability and surface tension of the GDL using the equation-of-state approach.

method was used. The best fit is associated with the values of γ_{sv} = 19.8 mJ m^{-2} and β = 0.00005398. Eq. (14) with the known surface tension value of water can then be used to obtain the internal contact angle of water, i.e., θ=98.5° (deg.). It is clear that the values obtained from the equation-of-state approach is in agreement with those obtained from the Owens–Wendt approach.

5. Summary

The knowledge of the surface properties of the GDL is of utmost importance in the study of water management in PEM fuel cells. Most studies conducted on the wettability of the GDL measure the external contact angle which does not describe the capillary forces acting on the water inside the pores. These methods depend on the surface roughness more than on the material composition of the GDL. As a result, the measured contact angle is larger than the contact angle of water on a pure PTFE surface. In this paper, the internal contact angle values of several pure liquids were determined by fitting a general form of Washburn's equation to the experimental data obtained from a height-based capillary penetration technique. The contact angle values were used to determine the wettability and surface energy of the GDL using two different approaches: the Owens–Wendt surface components and the equation-of-state approaches. The values of the GDL surface tension and the contact angle of water obtained from these two methods agree very well.

Acknowledgements

This work was supported by the Natural Science and Engineering Research Council (NSERC) of Canada. Financial support through the UBC Okanagan Undergraduate Student Research Award (USRA) (B.R.F.) is gratefully acknowledged.

References

[1] H. Li, Y. Tang, Z. Wang, Z. Shi, S. Wu, D. Song, J. Zhang, K. Fatih, J. Zhang, H. Wang, Z. Liu, R. Abouatallah, A. Mazza, J. Power Sources 178 (2008) 103–117.
[2] S. Litster, D. Sinton, N. Djilali, J. Power Sources 154 (2006) 95–105.
[3] D. Natarajan, T. Van Nguyen, J. Power Sources 115 (2003) 66–80.
[4] A. Su, F. Weng, C. Hsu, Y. Chen, Int. J. Hydrogen Energy 31 (2006) 1031–1039.
[5] K. Tüber, D. Pócza, C. Hebling, J. Power Sources 124 (2003) 403–414.
[6] F. Weng, A. Su, C. Hsu, C. Lee, J. Power Sources 157 (2006) 674–680.
[7] T. Berning, N. Djilali, J. Power Sources 124 (2003) 440–452.
[8] J. Larminie, A. Dicks, Fuel Cell Systems Explained, 2nd ed., John Wiley & Sons, England, 2003.
[9] S. Litster, D. Sinton, N. Djilali, J. Power Sources 154 (2005) 95–105.
[10] S. Park, B.N. Popov, Fuel 88 (2009) 2068–2073.
[11] U. Pasaogullari, C.-Y. Wang, K.S. Chen, J. Electrochem. Soc. 152 (2005) A1574–A1582.
[12] D. Wood, J. Davey, F. Garzon, P. Atanassov, R. Borup, Proceedings of the 206th Meeting of the Electrochemical Society, Hawaii, Honolulu, 2004.
[13] C. Lim, C.Y. Wang, Electrochim. Acta 49 (2004) 4149–4156.
[14] J. Benziger, J. Nehlsen, J.D. Blackwell, T. Brennan, J. Itescu, J. Membr. Sci. 261 (2005) 98–106.
[15] R. Borup, J. Davey, D. Wood, F. Garzon, M. Inbody, D. Guidry, DOE Hydrogen Program Rev. (2005).
[16] J.-H. Pai, J.-H. Ke, H.-F. Huang, C.-M. Lee, J.-M. Zen, F.-S. Shieu, J. Power Sources 161 (2006) 275–281.
[17] J.T. Gostick, M.A. Ioannidis, M.W. Fowler, M.D. Pritzker, J. Power Sources 173 (2007) 277–290.
[18] M.S. Yazici, F. Frate, R. Wayne, Perforated flexible graphite gas diffusion layers: processing, properties and performance, in: Fuel Cell Seminar, 2006 (abstract 655).
[19] V. Gurau, M.J. Bluemle, E.S. De Castro, Y.-M. Tsou, J.A. Mann, T.A. Zawodzinski, J. Power Sources 160 (2006) 1156–1162.
[20] A. Hamraoui, T. Nylander, J. Colloid Interface Sci. 250 (2002) 415–421.
[21] B.R. Friess, M. Shahraeeni, M. Hoorfar, Proceedings of 2008 AIChE Conference, Philadelphia, USA, 2008.
[22] L. Labajos-Broncano, M.L. González-Martín, J.M. Bruque, C.M. González-García, J. Colloid Interface Sci. 234 (2001) 79–83.
[23] J.J. Jasper, J. Phys. Chem. Ref. Data 1 (1972).
[24] K. Grundke, A. Augsburg, J. Adhes. Sci. Technol. 14 (1999) 765–775.
[25] J. Tröger, K. Lunkwitz, K. Grundke, B. Wolfgang, Physiochem. Eng. Aspects 134 (1997) 299–304.8.
[26] K. Grundke, T. Bogumil, T. Gietzelt, H.-J. Jacobasch, D.Y. Kwok, A.W. Neumann, Prog. Colloid Polym. Sci. 101 (1996) 58–68.
[27] S. Wu, Polymer Interface and Adhesion, Marcel Dekker Inc., New York, 1982.
[28] W. Sun, Y. Ya-xiang, Optimization Theory and Methods, Springer, New York, 2006.
[29] D.Y. Kwok, A.W. Neumann, Prog. Colloid Polym. Sci. 109 (1998) 170–184.